

Isothermal compressibility and effects of multibody molecular interactions in a strongly interacting ultracold Fermi gas

Daichi Kagamihara ¹, Ryohei Sato,² Koki Manabe,² Hiroyuki Tajima ³ and Yoji Ohashi ²

¹*Department of Physics, Kindai University, Higashi-Osaka, Osaka 577-8502, Japan*

²*Department of Physics, Keio University, 3-14-1 Hiyoshi, Kohoku-ku, Yokohama 223-8522, Japan*

³*Department of Physics, Graduate School of Science, The University of Tokyo, Tokyo 113-0033, Japan*



(Received 6 June 2022; accepted 17 August 2022; published 7 September 2022)

We theoretically investigate the isothermal compressibility κ_T in the normal state of an ultracold Fermi gas. Including pairing fluctuations, as well as preformed-pair formations, within the framework of the self-consistent T -matrix approximation, we evaluate the temperature dependence of this thermodynamic quantity over the entire BCS (Bardeen-Cooper-Schrieffer)-BEC (Bose-Einstein condensation) crossover region. While κ_T in the weak-coupling BCS regime is dominated by Fermi atoms near the Fermi surface, correlations between tightly bound Cooper-pair molecules are found to play crucial roles in the strong-coupling BEC regime. In the latter region, besides a two-body molecular interaction, a three-body one is shown to sizably affect κ_T near the superfluid phase-transition temperature. Our results indicate that the strong-coupling BEC regime of an ultracold Fermi gas would provide a unique opportunity to study multibody correlations between Cooper-pair molecules.

DOI: [10.1103/PhysRevA.106.033308](https://doi.org/10.1103/PhysRevA.106.033308)

I. INTRODUCTION

A pairing interaction between fermions and the resulting Cooper-pair formation are essential ingredients in all Fermi superfluids [1]. Particularly in ^{40}K and ^6Li Fermi gases [2–5], many-body quantum phenomena originating from a strong pairing interaction have attracted much attention [6–10], in connection to the BCS (Bardeen-Cooper-Schrieffer)-BEC (Bose-Einstein condensation) crossover phenomenon [11–21]: in these Fermi atomic gases, a pairing interaction associated with a Feshbach resonance is tunable by adjusting an external magnetic field [22]. Using this advantage, one can continuously change the character of a Fermi superfluid, from the weak-coupling BCS-type to BEC of tightly bound molecules, with increasing the interaction strength. In the intermediate coupling regime, normal-state properties are dominated by fluctuating preformed Cooper pairs, where various interesting many-body phenomena have been discussed both experimentally [23–39] and theoretically [40–65].

Besides the pairing interaction between fermions, the BCS-BEC crossover phenomenon also provides a unique opportunity to study interactions between Cooper-pair molecules in the strong-coupling BEC regime [14–16,66–70]. Since the ordinary BCS model (which can well describe ^{40}K and ^6Li Fermi gases) only involves an interatomic interaction, such *molecular* interactions are mediated by unpaired Fermi atoms, as shown in Fig. 1(a). Indeed, this diagram is known to give an interpair repulsion, being characterized by the s -wave molecular scattering length $a_B = 2a_s$ [14–16,70,71], where $a_s > 0$ is the s -wave atomic scattering length in the BEC regime. For the value of a_B , Pieri and Strinati [66] pointed out that it becomes small by about the factor three, when multiscattering processes of the two-body molecular interaction are taken

into account. Petrov and co-workers [67,68] exactly solved a four-fermion problem, to give $a_B \simeq 0.6a_s$. Brodsky and co-workers [72] rederived this exact molecular scattering length by using a diagrammatic technique. It has also been shown by a renormalization group analysis that many-body corrections lead to a temperature-dependent molecular interaction near the superfluid phase-transition temperature T_c [69].

Although a pairing interaction between fermions is, of course, essentially important in Fermi superfluids, correlations between Cooper pairs also play a crucial role in the superfluid state: in a Bose gas, the superfluid state is known to be unstable against an attractive interaction between bosons [73,74]. Thus the interaction must be repulsive for a Bose superfluid to be stable. In a stable Bose superfluid, the velocity v_ϕ of the collective Bogoliubov phonon is directly related to the Bose-Bose repulsion $U_B = 4\pi a_B/M_B$ as [73,74]

$$v_\phi = \sqrt{\frac{U_B N_c}{M_B}}, \quad (1)$$

where N_c is the Bose condensate fraction and M_B is a boson mass. (We set $\hbar = k_B = 1$ and the system volume V is taken to be unity throughout this paper.) Thus, if an interaction between Cooper-pair “bosons” was attractive, the Fermi superfluid could not stably exist there. The observed sound velocity in the BEC regime of a superfluid ^6Li gas agrees well with Eq. (1) with $a_B = 0.6a_s > 0$ [75], which means that the molecular interaction is fortunately *repulsive* there.

In BCS-BEC crossover physics, the molecular interaction in the BEC regime has so far mainly been discussed within the *two-body* level [14–16,66–70]. However, as a simple extension of Fig. 1(a), we can also expect, for example,

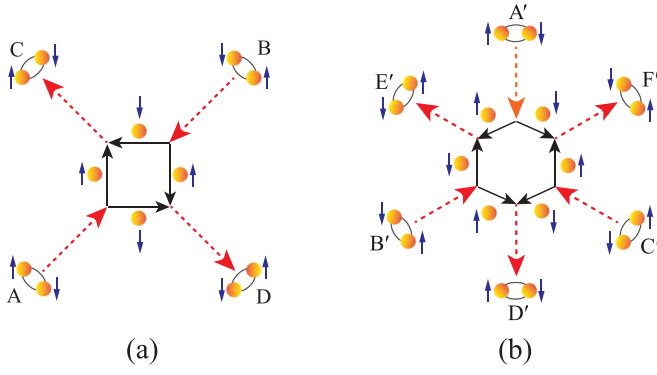


FIG. 1. Molecular interactions mediated by unpaired Fermi atoms in the strong-coupling BEC regime. (a) Two-body component. (b) Three-body component. The dashed (solid) line describes a bound molecule (dissociated Fermi atom). The pseudospin symbols $\sigma = \uparrow, \downarrow$ describe two atomic hyperfine states forming a Cooper pair. In panels (a) and (b), incident molecules (A, B, A', B', C') dissociate into four or six Fermi atoms, which are followed by recombination into outgoing molecules (C, D, D', E', F').

the *three-body* molecular interaction illustrated in Fig. 1(b), which is mediated by six unpaired Fermi atoms. At a glance, since molecular interactions in Fig. 1 are always accompanied by virtual dissociation of molecules in the intermediate state, the resulting interaction seems weaker for a higher-body component. However, the importance of such multibody molecular interactions is still unclear. Because three-body interactions have also been discussed in various research fields, such as nuclear physics [76,77], as well as neutron-star physics [78], systematic studies on multibody molecular correlations by using the high tunability of ultracold Fermi gases would make an impact on these research fields.

The purpose of this paper is to examine how multibody molecular interactions affect the strong-coupling properties of an ultracold Fermi gas. For this purpose, this paper deals with the isothermal compressibility κ_T . To explain the reason for this choice, we recall that, as shown in Fig. 2, the isothermal compressibility in an ideal Bose gas,

$$\begin{aligned} \kappa_T^{\text{B},0}(T) &= \frac{1}{N_B^2} \left(\frac{\partial N_B}{\partial \mu_B} \right)_T \\ &= \frac{1}{N_B^2} \left(\frac{\partial}{\partial \mu_B} \sum_q \frac{1}{e^{[\varepsilon_q^{\text{B}} - \mu_B]/T} - 1} \right)_T, \end{aligned} \quad (2)$$

diverges at the Bose-Einstein condensation temperature T_{BEC} because of $\mu_B \rightarrow 0$ as

$$\kappa_T^{\text{B},0}(T_{\text{BEC}}) = \frac{1}{N_B^2 T_{\text{BEC}}} \sum_q \text{cosech}^2 \left(\frac{\varepsilon_q^{\text{B}}}{2T_{\text{BEC}}} \right) \rightarrow \infty. \quad (3)$$

Here, $\varepsilon_q^{\text{B}} = \mathbf{q}^2/(2M_B)$ is the kinetic energy of a boson, N_B the number of bosons, and μ_B the Bose chemical potential. This divergence at T_{BEC} is absent in the presence of an *s*-wave Bose-Bose repulsion $U_B > 0$. Indeed, treating U_B within the

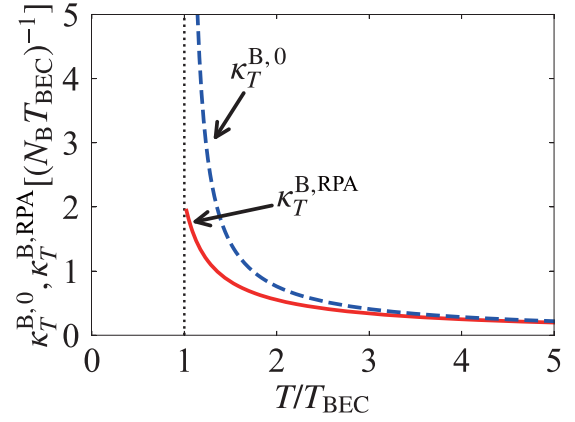


FIG. 2. Isothermal compressibility in a Bose gas as a function of temperature. $\kappa_T^{\text{B},0}$ and $\kappa_T^{\text{B,RPA}}$, respectively, show the cases of an ideal Bose gas given in Eq. (2) and a repulsively interacting Bose gas given in Eq. (5). In the latter, we take $U_B N_B = 0.25 T_{\text{BEC}}$ and the Bose-Bose repulsion U_B is treated within the Hartree Fock RPA. N_B is the number of bosons and T_{BEC} is the BEC phase-transition temperature.

Hartree-Fock approximation, one has

$$\begin{aligned} \kappa_T^{\text{B,RPA}}(T) &= \frac{1}{N_B^2} \left(\frac{\partial}{\partial \mu_B} \sum_q \frac{1}{e^{[\varepsilon_q^{\text{B}} + 2U_B N_B - \mu_B]/T} - 1} \right)_T \\ &= \kappa_T^{\text{B},0}(T) \left[1 - 2U_B \left(\frac{\partial N_B}{\partial \mu_B} \right)_T \right]. \end{aligned} \quad (4)$$

Equation (4) gives the following expression for the isothermal compressibility in the random-phase approximation (RPA):

$$\kappa_T^{\text{B,RPA}}(T) = \frac{\kappa_T^{\text{B},0}(T)}{1 + 2U_B N_B^2 \kappa_T^{\text{B},0}(T)}. \quad (5)$$

Although the bare isothermal compressibility $\kappa_T^{\text{B},0}$ diverges at T_{BEC} , Eq. (5) converges to give (see also Fig. 2)

$$\kappa_T^{\text{B,RPA}}(T_{\text{BEC}}) = \frac{1}{2U_B N_B^2}. \quad (6)$$

This indicates that the isothermal compressibility near the superfluid instability is sensitive to a Bose-Bose interaction. Thus similar sensitivity is also expected in the BEC regime of an ultracold Fermi gas where most Fermi atoms form tightly bound molecules.

To include strong-coupling effects in the BCS-BEC crossover region, this paper employs the self-consistent *T*-matrix approximation (SCTMA). References [15,16] showed that the SCTMA gives the molecular scattering length $a_B = 2a_s$. It has also been shown that the calculated κ_T in the SCTMA agrees well with the observed one in a ${}^6\text{Li}$ unitary Fermi gas [32,33,57]. Thus the SCTMA is expected to be suitable for our purpose. We briefly note that another well-known BCS-BEC crossover theory called the *T*-matrix approximation (TMA) [79] cannot deal with molecular correlations in the normal state [80]. Using the SCTMA scheme, we show that a *three-body* molecular interaction sizably affects κ_T in the BEC regime. As mentioned previously, although the SCTMA cannot reproduce the exact value of the molecular scattering a_B [67,68], this strong-coupling scheme is found to

still provide useful information about how multibody molecular interactions work in the BEC regime of an ultracold Fermi gas.

This paper is organized as follows. In Sec. II, we explain our formulation to evaluate κ_T in the SCTMA [15,16]. We show our results in Sec. III. In the BEC regime, we evaluate the effects of two-body and three-body molecular interactions from the comparison of our SCTMA result with the isothermal compressibility in an assumed weakly interacting molecular Bose gas. We also compare our result with the recent experiment on a ^6Li unitary Fermi gas [34].

II. FORMULATION

We consider a two-component uniform Fermi gas, described by the BCS Hamiltonian,

$$H = \sum_{p,\sigma} \xi_p c_{p,\sigma}^\dagger c_{p,\sigma} - U \sum_{p,p',q} c_{p+q/2,\uparrow}^\dagger c_{-p+q/2,\downarrow}^\dagger c_{-p'+q/2,\downarrow} c_{p'+q/2,\uparrow}. \quad (7)$$

Here, $c_{p,\sigma}^\dagger$ is the creation operator of a Fermi atom with pseudospin $\sigma = \uparrow, \downarrow$, describing two atomic hyperfine states. The kinetic energy $\xi_p = \varepsilon_p - \mu = p^2/(2m) - \mu$ is measured from the Fermi chemical potential μ , where m is an atomic mass. $-U$ (< 0) is a contact-type s -wave pairing interaction between Fermi atoms, which is assumed to be tunable by adjusting the threshold energy of a Feshbach resonance [22]. We emphasize that Eq. (7) has no term describing any molecular interaction.

We conveniently measure the strength of the pairing interaction in terms of the s -wave scattering length a_s , which is related to the bare interaction $-U$ as

$$\frac{4\pi a_s}{m} = - \frac{U}{1 - U \sum_p^{p_c} \frac{1}{2\varepsilon_p}}, \quad (8)$$

where p_c is a momentum cutoff. The weak-coupling BCS regime and strong-coupling BEC regime are then characterized by $(k_F a_s)^{-1} \lesssim -1$ and $(k_F a_s)^{-1} \gtrsim +1$, respectively (where k_F is the Fermi momentum). The region $-1 \lesssim (k_F a_s)^{-1} \lesssim +1$ is sometimes referred to as the (BCS-BEC) crossover region in the literature.

Strong-coupling corrections to single-particle properties of the system are conveniently described by the self-energy $\Sigma(\mathbf{p}, i\omega_n)$ in the dressed Fermi single-particle thermal Green's function,

$$G(\mathbf{p}, i\omega_n) = \frac{1}{G_0(\mathbf{p}, i\omega_n)^{-1} - \Sigma(\mathbf{p}, i\omega_n)}, \quad (9)$$

where

$$G_0(\mathbf{p}, i\omega_n) = \frac{1}{i\omega_n - \xi_p} \quad (10)$$

is the bare Green's function, with ω_n being the fermion Matsubara frequency. In the SCTMA, $\Sigma(\mathbf{p}, i\omega_n)$ is diagram-

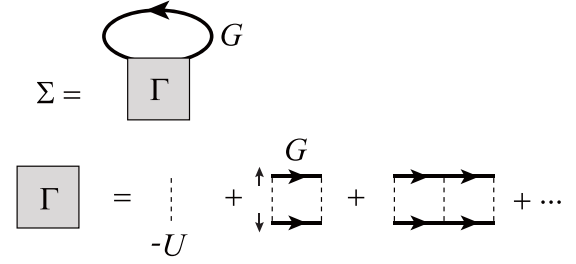


FIG. 3. SCTMA self-energy correction Σ . The solid line represents the dressed single-particle thermal Green's function G in Eq. (9). The dotted line is a pairing interaction $-U$. Γ is the particle-particle scattering matrix in Eq. (12).

matically described as Fig. 3, which gives

$$\Sigma(\mathbf{p}, i\omega_n) = T \sum_{q, \nu_n} \Gamma(\mathbf{q}, i\nu_n) G(\mathbf{q} - \mathbf{p}, i\nu_n - i\omega_n). \quad (11)$$

Here, ν_n is the boson Matsubara frequency and

$$\Gamma(\mathbf{q}, i\nu_n) = - \frac{U}{1 - U\Pi(\mathbf{q}, i\nu_n)} = \frac{4\pi a_s}{m} \frac{1}{1 + \frac{4\pi a_s}{m} \left[\Pi(\mathbf{q}, i\nu_n) - \sum_p \frac{1}{2\varepsilon_p} \right]} \quad (12)$$

is the SCTMA particle-particle scattering matrix, describing pairing fluctuations. We briefly note that $\Gamma(\mathbf{q}, i\nu_n)$ is directly related to a molecular Bose Green's function deep inside the BEC regime [15,16]. In Eq. (12),

$$\Pi(\mathbf{q}, i\nu_n) = T \sum_{p, \omega_n} G(\mathbf{p}, i\omega_n) G(\mathbf{q} - \mathbf{p}, i\nu_n - i\omega_n) \quad (13)$$

is the pair-correlation function. Although Eq. (13) involves the ultraviolet divergence, it is actually canceled out by the term $\sum_p (1/2\varepsilon_p)$ in Eq. (12) [15,16].

Here, we explain how the two-body molecular interaction is obtained in the present SCTMA scheme [15,16]: since Γ in Eq. (12) consists of the dressed Green's function G , it involves the diagram shown in Fig. 4(a). Then, deforming this diagram as Fig. 4(b), and simply regarding the shaded parts as molecular Bose propagators, one finds that Fig. 4(b) has the same diagrammatic structure as the Hartree self-energy correction to a Bose Green's function shown in Fig. 4(c). This two-body Bose-Bose interaction ($\equiv \bar{U}_B^{2\text{-body}}$) is mediated by four unpaired fermions A to D in Fig. 4(b) and the diagrammatic structure is the same as Fig. 1(a). References [15,16] evaluated this molecular interaction in the BEC regime to give

$$\bar{U}_B^{2\text{-body}} = \frac{4\pi(2a_s)}{2m}. \quad (14)$$

Recently, the existence of a correction to Eq. (14) in the SCTMA has been pointed out [81]. We will later discuss this from the viewpoint of three-body molecular interaction.

We briefly note that the TMA is obtained by replacing all the dressed Green's function G in Eqs. (11) and (13) with the bare one G_0 in Eq. (10). The resulting TMA particle-particle

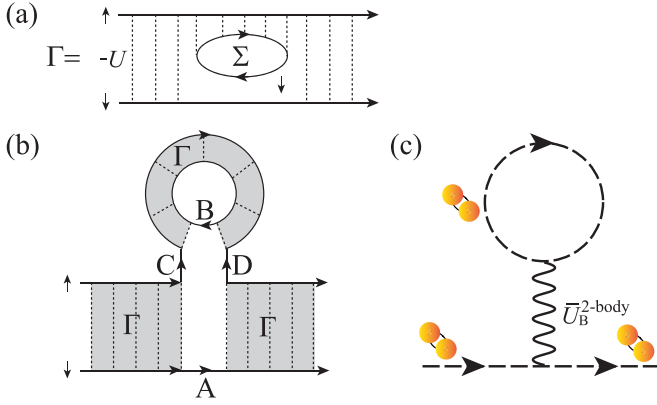


FIG. 4. Effective two-body molecular interaction involved in the SCTMA [15,16]. Since the SCTMA particle-particle scattering matrix Γ in Eq. (12) consists of the dressed Green's function G (solid line) and the pairing interaction $-U$ (dotted line), Γ involves the diagrams shown in panel (a). Without changing the topology, this diagram can be deformed as panel (b). Then, regarding each shaded part in panel (b) as a molecular Bose propagator, one may view the diagram in panel (b) as the Hartree self-energy correction to the molecular Bose Green's function shown in panel (c). In panel (c), the dashed line is the molecular Bose Green's function and the molecular interaction $\bar{U}_B^{2\text{-body}}$ corresponds to the four fermion lines A to D in panel (b). The diagrammatic structure giving $\bar{U}_B^{2\text{-body}}$ is the same as Fig. 1(a).

scattering matrix does not involve the diagram in Fig. 4(a). As a result, the noninteracting molecular Bose Green's function is only obtained in this scheme.

The superfluid phase-transition temperature T_c is conveniently determined from the Thouless criterion [82], stating that the system achieves the superfluid instability when the particle-particle scattering matrix Γ in Eq. (12) has a pole at $q = v_n = 0$, which gives

$$1 = -\frac{4\pi a_s}{m} \left[\Pi(0, 0) - \sum_p \frac{1}{2\varepsilon_p} \right]. \quad (15)$$

We actually solve the T_c equation (15), together with the equation for the total number N of Fermi atoms,

$$N = 2T \sum_{\mathbf{p}, \omega_n} G(\mathbf{p}, i\omega_n), \quad (16)$$

to self-consistently determine T_c and $\mu(T_c)$. Above T_c , we only deal with Eq. (16) to evaluate $\mu(T > T_c)$. We briefly show in Fig. 5 the SCTMA solutions for T_c and $\mu(T_c)$ that will be used in evaluating κ_T . For computational details, see Appendix A.

Once T_c and $\mu(T_c)$, as well as $\mu(T > T_c)$, are determined, we then evaluate the isothermal compressibility κ_T from the following thermodynamic relation:

$$\kappa_T = \frac{1}{N^2} \left(\frac{\partial N}{\partial \mu} \right)_T. \quad (17)$$

(Note that the system volume is taken to be unity in this paper.) Substituting the number equation (16) into Eq. (17), one obtains

$$\kappa_T = -\frac{2T}{N^2} \sum_{\mathbf{p}, \omega_n} G^2(\mathbf{p}, i\omega_n) \Lambda(\mathbf{p}, i\omega_n), \quad (18)$$

where the three-point vertex $\Lambda(\mathbf{p}, i\omega_n)$ obeys the equation

$$\begin{aligned} \Lambda(\mathbf{p}, i\omega_n) &= 1 - \frac{\partial \Sigma(\mathbf{p}, i\omega_n)}{\partial \mu} \\ &= 1 + T \sum_{\mathbf{q}, \nu_n} \Gamma(\mathbf{q}, i\nu_n) G^2(\mathbf{q} - \mathbf{p}, i\nu_n - i\omega_n) \Lambda(\mathbf{q} - \mathbf{p}, i\nu_n - i\omega_n) \\ &\quad - 2T^2 \sum_{\mathbf{p}', \omega'_n} \sum_{\mathbf{q}, \nu_n} G(\mathbf{q} - \mathbf{p}, i\nu_n - i\omega_n) \Gamma^2(\mathbf{q}, i\nu_n) G^2(\mathbf{p}', i\omega'_n) G(\mathbf{q} - \mathbf{p}', i\nu_n - i\omega'_n) \Lambda(\mathbf{p}', i\omega'_n). \end{aligned} \quad (19)$$

Equations (18) and (19) are diagrammatically described as Figs. 6(a) and 6(b), respectively.

When we evaluate κ_T from Eq. (18), we have to self-consistently solve Eq. (19) to determine the vertex correction Λ . In this paper, to avoid this complicated procedure, we numerically carry out the μ derivative in Eq. (17) to obtain κ_T . We will use Eqs. (18) and (19) in Sec. III B, where we examine how molecular interactions affect κ_T .

III. ISOTHERMAL COMPRESSIBILITY AND EFFECTS OF MOLECULAR INTERACTIONS

A. Isothermal compressibility in the BCS-BEC crossover region

Figure 7(a) shows the SCTMA isothermal compressibility κ_T in the normal state of an ultracold Fermi gas in the

BCS-BEC crossover region. As expected from the nonzero molecular scattering length $a_B = 2a_s$ [15,16], the calculated κ_T converges at T_c in the whole BCS-BEC crossover region, especially in the BEC regime. This is quite different from the TMA result shown in Fig. 7(b), where κ_T always diverges at T_c . In the TMA case, the divergence in the BEC regime is due to the ignorance of the molecular interaction. [For more details about the singular behavior seen in Fig. 7(b), see Appendix B.] Because of this difference, as shown in Fig. 8, while the SCTMA well explains the experimental result on a ^6Li unitary Fermi gas, the TMA overestimates κ_T , when $T/T_F \lesssim 0.4$ (where T_F is the Fermi temperature).

Figure 9(a) shows $\kappa_T(T_c)$ in the SCTMA. In the weak-coupling BCS regime [$(k_F a_s)^{-1} \lesssim -1$], system properties are dominated by Fermi atoms, so that κ_T is well described by

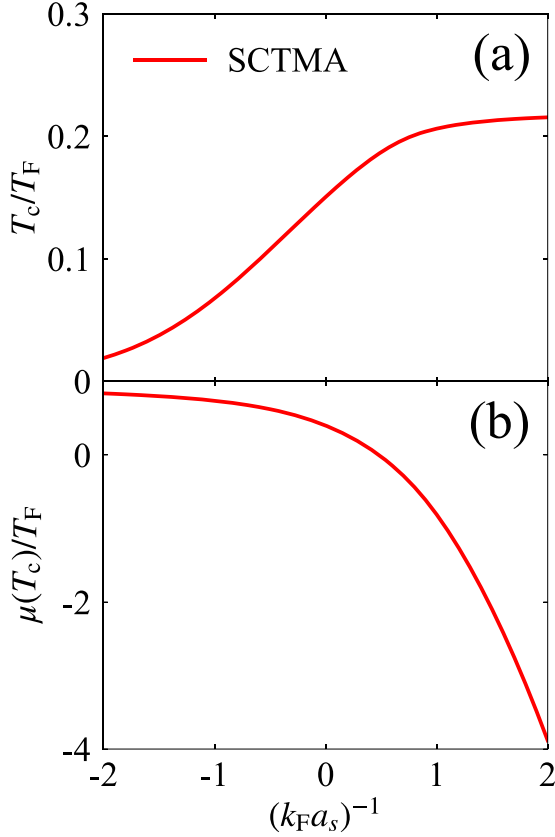


FIG. 5. SCTMA self-consistent solutions for (a) T_c and (b) $\mu(T_c)$. T_F is the Fermi temperature.

that in a free Fermi gas,

$$\begin{aligned} \kappa_T^F(T_c) &\equiv \frac{2}{N^2} \frac{\partial}{\partial \mu} \sum_p \frac{1}{e^{(\varepsilon_p - \tilde{\mu})/T_c} + 1} \\ &= \frac{1}{2T_c N^2} \left(\frac{\partial \tilde{\mu}}{\partial \mu} \right) \sum_p \operatorname{sech}^2 \left(\frac{\varepsilon_p - \tilde{\mu}}{2T_c} \right). \end{aligned} \quad (20)$$

Here, $\tilde{\mu} = \tilde{k}_F^2/(2m)$ is the effective Fermi chemical potential, where the effective Fermi momentum \tilde{k}_F is determined from the pole equation of the analytic-continued dressed single-particle Green's function $G(\mathbf{p}, i\omega_n \rightarrow \omega + i\delta)$ at $\omega = 0$

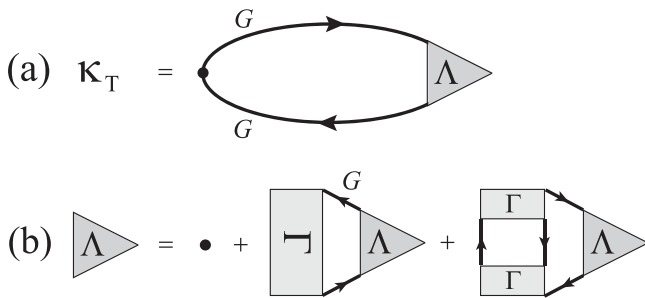


FIG. 6. (a) Diagrammatic representation of isothermal compressibility κ_T in Eq. (18). The solid circle is the bare density vertex and Λ the three-point vertex correction. (b) Diagrammatic equation for Λ in the SCTMA. Γ is the particle-particle scattering matrix in Eq. (12).

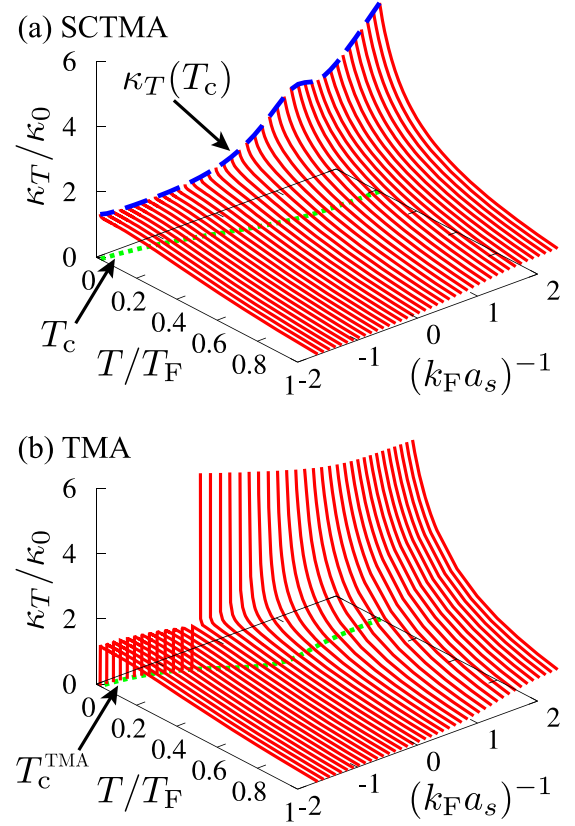


FIG. 7. Calculated isothermal compressibility κ_T in the normal state of an ultracold Fermi gas in the BCS-BEC crossover region. (a) SCTMA. (b) TMA. In panel (b), κ_T always diverges at the superfluid phase-transition temperature T_c^{TMA} evaluated in the TMA. (Note that T_c^{TMA} does not equal T_c obtained in the SCTMA.) It diverges positively (negatively) when $(k_F a_s)^{-1} \gtrless -0.79$ [$(k_F a_s)^{-1} \lesssim -0.79$]. $\kappa_0 = 3m/(k_F^2 N)$ is the isothermal compressibility in a free Fermi gas at $T = 0$.

[54,83],

$$\frac{\tilde{k}_F^2}{2m} - \mu + \operatorname{Re}[\Sigma(\tilde{\mathbf{k}}_F, i\omega_n \rightarrow \omega + i\delta = 0 + i\delta)] = 0, \quad (21)$$

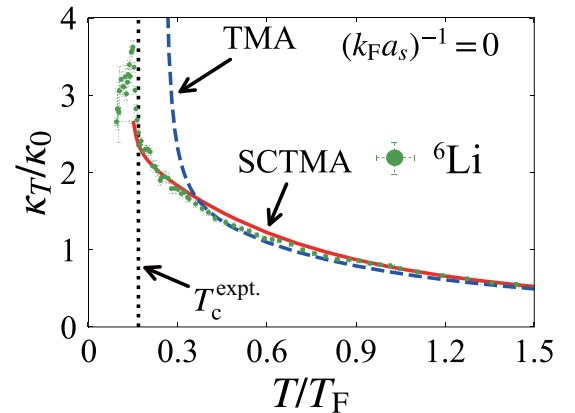


FIG. 8. Comparison of our theoretical results (SCTMA and TMA) with the recent experiment on a ${}^6\text{Li}$ unitary Fermi gas [34]. T_c^{expt} is the superfluid phase-transition temperature which is experimentally determined in Ref. [34].

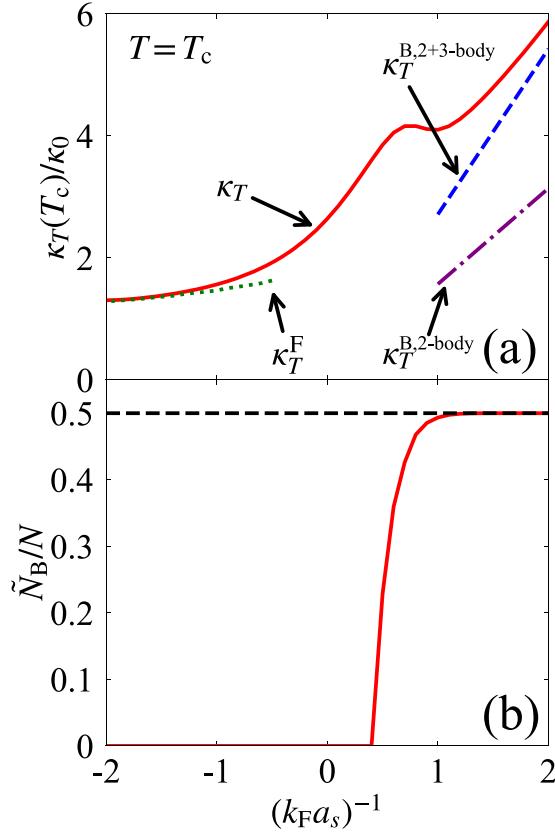


FIG. 9. (a) SCTMA isothermal compressibility κ_T at T_c . κ_T^F is the isothermal compressibility in a free Fermi gas given in Eq. (20). $\kappa_T^{B,2\text{-body}}$ is the isothermal compressibility in an assumed molecular Bose gas given in Eq. (6), where $M_B = 2m$, $N_B = N/2$, and $U_B = \bar{U}_B^{2\text{-body}} = 4\pi(2a_s)/M_B$. $\kappa_T^{B,2+3\text{-body}}$ includes the effects of two-body and three-body molecular interactions, given in Eq. (36). (b) The number \tilde{N}_B of (quasi)stable molecules at T_c .

with δ being an infinitesimally small positive number. Because the function $\text{sech}^2[(\varepsilon_p - \tilde{\mu})/2T_c]$ in Eq. (20) selectively extracts the contribution around the effective Fermi level $\varepsilon_p = \tilde{\mu}$, $\kappa_T(T_c)$ in this regime is dominated by Fermi atoms near this effective Fermi surface.

Starting from the weak-coupling BCS regime, one sees in Fig. 9(a) that $\kappa_T(T_c)$ increases with increasing the strength of the pairing interaction. This behavior seen in the BCS side $[(k_F a_s)^{-1} \lesssim 0]$ is simply due to the well-known property that an attractive Fermi-Fermi interaction enhances the isothermal compressibility.

However, Fig. 9(a) shows that the increase of $\kappa_T(T_c)$ is not monotonic, but it exhibits a hump structure around $(k_F a_s)^{-1} = 0.7$. Regarding this, estimating the number \tilde{N}_B of (quasi)stable molecules [84], we find in Fig. 9(b) that \tilde{N}_B rapidly increases around $(k_F a_s)^{-1} = 0.7$. (We explain how to estimate \tilde{N}_B in Appendix C.) Thus the hump structure around $(k_F a_s)^{-1} = 0.7$ is considered to be related to the change of dominant particles, from Fermi atoms to Bose molecules [85].

When we simply regard the right region of this hump $[(k_F a_s)^{-1} \gtrsim +1]$ as a gas of weakly interacting $N/2$ Bose molecules with the *two-body* molecular repulsion $\bar{U}_B^{2\text{-body}}$ in Eq. (14), Eq. (6) with $U_B = \bar{U}_B^{2\text{-body}}$ ($\equiv \kappa_T^{B,2\text{-body}}$) cannot ex-

plain $\kappa_T(T_c)$, as shown in Fig. 9(a). In the next subsection, we will show that a three-body molecular interaction resolves this discrepancy.

B. Effects of three-body molecular interaction on κ_T in the BEC regime

To examine how molecular interactions affect κ_T in the BEC regime, we rewrite Eq. (18) by substituting Eq. (19) into this equation. The resulting expression $\kappa_T = \sum_{j=1}^3 \kappa_T^{(j)}$ consists of three terms, where

$$\kappa_T^{(1)} = -\frac{2T}{N^2} \sum_{\mathbf{p}, \omega_n} G^2(\mathbf{p}, i\omega_n), \quad (22)$$

$$\begin{aligned} \kappa_T^{(2)} = & -\frac{2T^2}{N^2} \sum_{\mathbf{p}, \omega_n} \sum_{\mathbf{q}, v_n} G^2(\mathbf{p}, i\omega_n) \Gamma(\mathbf{q}, iv_n) \\ & \times G^2(\mathbf{q} - \mathbf{p}, iv_n - i\omega_n) \Lambda(\mathbf{q} - \mathbf{p}, iv_n - i\omega_n), \end{aligned} \quad (23)$$

$$\begin{aligned} \kappa_T^{(3)} = & \frac{4T^3}{N^2} \sum_{\mathbf{p}, \omega_n} \sum_{\mathbf{p}', \omega'_n} \sum_{\mathbf{q}, v_n} G^2(\mathbf{p}, i\omega_n) \\ & \times G(\mathbf{q} - \mathbf{p}, iv_n - i\omega_n) \Gamma^2(\mathbf{q}, iv_n) \\ & \times G^2(\mathbf{p}', i\omega'_n) G(\mathbf{q} - \mathbf{p}', iv_n - i\omega'_n) \Lambda(\mathbf{p}', i\omega'_n). \end{aligned} \quad (24)$$

Among them, $\kappa_T^{(1)} + \kappa_T^{(2)}$ gives the ordinary RPA expression for the isothermal compressibility in a weakly interacting Fermi gas. Indeed, simply approximating Γ by the bare interaction $-U$ and ignoring the last term in Eq. (19), one obtains

$$\kappa_T^{(1)} + \kappa_T^{(2)} \simeq \frac{\kappa_T^{(1)}}{1 - \frac{UN^2}{2} \kappa_T^{(1)}}. \quad (25)$$

To evaluate Eq. (25) in the BEC regime, we recall that, deep inside the BEC regime, the Fermi chemical potential μ approaches [12,14–17]

$$\mu_{\text{BEC}} \equiv -\frac{1}{2ma_s^2}. \quad (26)$$

As a result, $|\mu|$ eventually becomes much larger than the SCTMA self-energy Σ involved in the dressed Green's function $G(\mathbf{p}, i\omega)$ in Eq. (9). In this case, one may ignore Σ compared to $\mu < 0$ in evaluating $\kappa_T^{(1)}$, giving

$$\begin{aligned} \kappa_T^{(1)} & \simeq -\frac{2T}{N^2} \sum_{\mathbf{p}, \omega_n} G_{\text{BEC}}^2(\mathbf{p}, i\omega_n) \\ & = \frac{1}{2TN^2} \sum_{\mathbf{p}} \text{sech}^2\left(\frac{\varepsilon_p + |\mu_{\text{BEC}}|}{2T}\right). \end{aligned} \quad (27)$$

Here, $G_{\text{BEC}}(\mathbf{p}, i\omega_n)$ has the same form as the bare Green's function $G_0(\mathbf{p}, i\omega_n)$ in Eq. (10), where the chemical potential μ is replaced by μ_{BEC} in Eq. (26). Equation (27), as well as Eq. (25), vanishes in the BEC limit ($\mu_{\text{BEC}} \rightarrow -\infty$), so that the isothermal compressibility in the BEC regime is dominated by $\kappa_T^{(3)}$ in Eq. (24).

Repeatedly substituting the three-point vertex Λ given in Eq. (19) into Eq. (24), one finds that $\kappa_T^{(3)}$ involves the diagrammatic series shown in Fig. 10(a). Using the fact that the particle-particle scattering matrix $\Gamma(0, 0)$ diverges at T_c , we

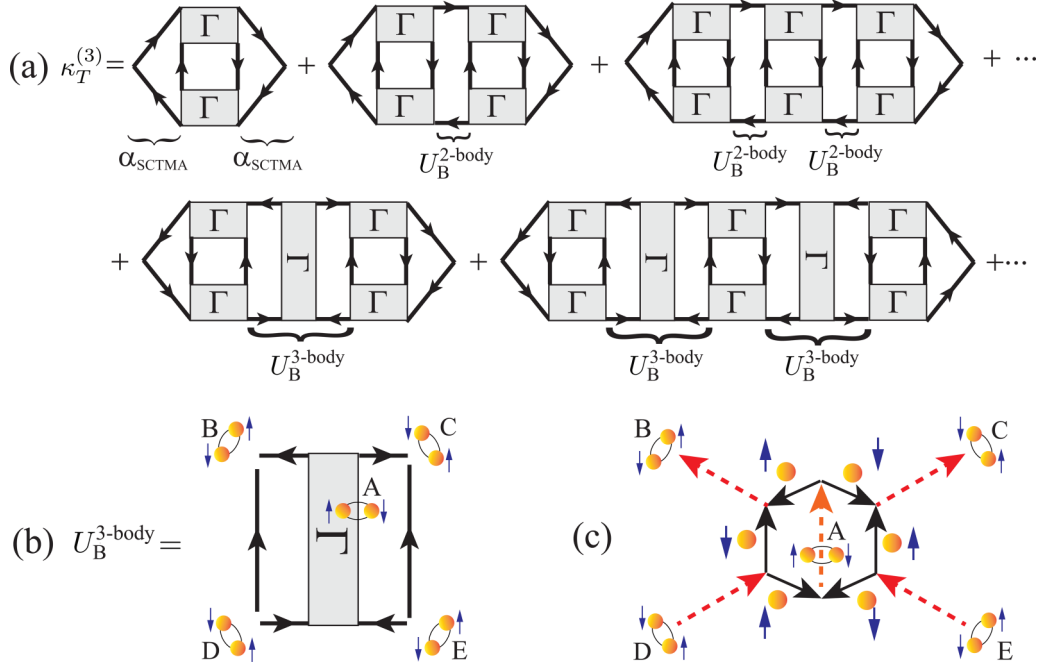


FIG. 10. (a) Diagrams involved in $\kappa_T^{(3)}$. When Γ is regarded as the molecular Green's function, the rectangular part being composed of four Fermi atoms (four solid lines) and the triangular part in the first line may be interpreted as the two-body molecular interaction ($= U_B^{2\text{-body}}$) and the three-point vertex ($= \alpha_{\text{SCTMA}}$) of the Bose isothermal compressibility, respectively. The diagrams in the second line involve $U_B^{3\text{-body}}$ shown in panel (b). We show in panel (c) that $U_B^{3\text{-body}}$ is obtained from the three-body molecular interaction in Fig. 1(b). Molecular propagators A to E in panel (b) correspond to those in panel (c).

approximately evaluate the first term ($\equiv \kappa_{T_0}^{(3)}$) in Fig. 10(a) as

$$\kappa_{T_0}^{(3)}(T_c) \simeq \frac{\alpha_{\text{SCTMA}}^2 T_c}{N^2} \sum_{\mathbf{q}, \nu_n} \Gamma^2(\mathbf{q}, i\nu_n), \quad (28)$$

where

$$\alpha_{\text{SCTMA}} = 2T_c \sum_{\mathbf{p}, \omega_n} G^2(\mathbf{p}, i\omega_n) G(-\mathbf{p}, -i\omega_n). \quad (29)$$

In the BEC regime, it has been shown that $\Gamma(\mathbf{q}, i\nu_n)$ at T_c is directly related to the Bose single-particle Green's function $G_B^{-1}(\mathbf{q}, i\nu_n) = i\nu_n - \varepsilon_q^B$ as [66,86]

$$\Gamma(\mathbf{q}, i\nu_n) = Z(\mathbf{q}, i\nu) G_B(\mathbf{q}, i\nu_n). \quad (30)$$

Here, the molecular mass M_B in the Bose kinetic energy $\varepsilon_q^B = q^2/2M_B$ equals $2m$ and

$$Z(\mathbf{q}, i\nu_n) = \frac{4\pi}{m^2 a_s} \left[1 + \sqrt{1 + \frac{-i\nu_n + \varepsilon_q^B}{E_{\text{bind}}}} \right], \quad (31)$$

where $E_{\text{bind}} = 1/(ma_s^2)$ is the binding energy of a two-body bound state. Substitution of Eq. (30) into Eq. (28) gives

$$\begin{aligned} \kappa_{T_0}^{(3)}(T_c) &\simeq \frac{\alpha_{\text{SCTMA}}^2 Z^2(0, 0) T_c}{N^2} \sum_{\mathbf{q}, \nu_n} G_B^2(\mathbf{q}, i\nu_n) \\ &\simeq \frac{1}{4(N/2)^2 T_c} \sum_{\mathbf{q}} \text{cosech}^2\left(\frac{\varepsilon_q^B}{2T_c}\right). \end{aligned} \quad (32)$$

In obtaining the last expression, we have approximated G involved in α_{SCTMA} to G_{BEC} . Equation (32), which diverges at T_c , is the same form as Eq. (3) with the boson number $N_B = N/2$.

The first line in Fig. 10(a) is the series of diagrams involving the two-body molecular interaction $U_B^{2\text{-body}}$ mediated by four unpaired fermions. Evaluating these diagrams in the same manner as $\kappa_{T_0}^{(3)}$, and adding them to Eq. (32), they reproduce $\kappa_T^{\text{B}, 2\text{-body}}$ plotted in Fig. 9(a):

$$\begin{aligned} \kappa_T^{\text{B}, 2\text{-body}}(T_c) &= \frac{\kappa_{T_0}^{(3)}(T_c)}{1 + 2U_B^{2\text{-body}} N_B^2 \kappa_{T_0}^{(3)}(T_c)} \\ &\rightarrow \frac{1}{2U_B^{2\text{-body}} N_B^2}. \end{aligned} \quad (33)$$

Here,

$$\begin{aligned} U_B^{2\text{-body}} &= Z^2(0, 0) T \sum_{\mathbf{p}, \omega_n} G_{\text{BEC}}^2(\mathbf{p}, i\omega_n) G_{\text{BEC}}^2(-\mathbf{p}, -i\omega_n) \\ &= \frac{4\pi(2a_s)}{M_B} \end{aligned} \quad (34)$$

just coincides with Eq. (14). Regarding this, we note that, while $\bar{U}_B^{2\text{-body}}$ in Eq. (14) is obtained from the Hartree self-energy in Fig. 4(c), $U_B^{2\text{-body}}$ in Eq. (34) is extracted from the RPA vertex correction to κ_T . This is a consequence of the present consistent treatment of the SCTMA self-energy Σ and the three-point vertex correction Λ .

The above analysis indicates that the difference between $\kappa_T(T_c)$ in the SCTMA and $\kappa_T^{B,2\text{-body}}(T_c)$ seen in Fig. 9(a) comes from the second line in Fig. 10(a), where each diagram has the part $U_B^{3\text{-body}}$ depicted in Fig. 10(b). When one again relates Γ to the molecular Bose Green's function in the BEC regime, $U_B^{3\text{-body}}$ is found to be obtained from the *three-body* molecular interaction given in Fig. 1(b), as shown in Fig. 10(c). Because the two of six external lines are contracted in Fig. 10(c), $U_B^{3\text{-body}}$ may be interpreted as a *three-body correction to the two-body molecular interaction*. Evaluating $U_B^{3\text{-body}}$ in the same manner as Eq. (34), one has, in the BEC regime at T_c ,

$$\begin{aligned} U_B^{3\text{-body}} &\simeq Z^2(\mathbf{0}, 0)T_c^2 \sum_{\mathbf{p}, \mathbf{p}', \omega_n, \omega'_n} G_{\text{BEC}}^2(\mathbf{p}, i\omega_n) \\ &\quad \times G_{\text{BEC}}(-\mathbf{p}, -i\omega_n)\Gamma(\mathbf{p} + \mathbf{p}', i\omega_n + i\omega'_n) \\ &\quad \times G_{\text{BEC}}^2(\mathbf{p}', i\omega'_n)G_{\text{BEC}}(-\mathbf{p}', -i\omega'_n) \\ &= -\frac{4\pi(0.842a_s)}{M_B}. \end{aligned} \quad (35)$$

For the derivation of Eq. (35), see Appendix D.

We comment on the sign of $U_B^{3\text{-body}}$ in Eq. (35): a two-body interaction between molecules is usually considered to be associated with the exchange of constituent Fermi atoms involved in molecules and consequently be repulsive due to the Pauli exclusion principle. Regarding this, Haussmann pointed out that scattering processes contributing to the molecular interaction can be classified into three classes [15]. The first class is the molecular scattering by a Fermi-Fermi interaction $-U$. The second class is the same as the first one except that the outgoing molecules are exchanged. The third class involves fermion exchange and this class gives a repulsive interaction due to the Pauli exclusion principle. Haussmann showed in the SCTMA that, while the third class gives Eq. (14) ($\propto a_s$), the other classes only give corrections in the subleading order with respect to a_s , by considering the first-order contribution of $-U$. Employing this classification, we find that $U_B^{3\text{-body}}$ in Eq. (35) belongs to the first class, because it is not accompanied by the fermion exchange. Because of this, the sign of $U_B^{3\text{-body}}$ is not attributed to the Pauli exclusion principle, in contrast to $U_B^{2\text{-body}} > 0$ in Eq. (34). $U_B^{3\text{-body}}$ becomes $O(a_s)$ due to the multiscattering processes with respect to $-U$, which is effectively described by the particle-particle scattering matrix Γ appearing in the center of Fig. 10(b), and the resulting sign of this correction becomes negative, as shown in Eq. (35).

Summing up the series of diagrams in both the first and second lines in Fig. 10(a), as well as diagrams involving both $U_B^{2\text{-body}}$ and $U_B^{3\text{-body}}$ (that are not explicitly shown in Fig. 10), we reach

$$\begin{aligned} \kappa_T^{B,2+3\text{-body}}(T_c) &= \frac{\kappa_{T0}^{(3)}(T_c)}{1 + 2[U_B^{2\text{-body}} + U_B^{3\text{-body}}]N_B^2\kappa_{T0}^{(3)}(T_c)} \\ &\rightarrow \frac{1}{2[U_B^{2\text{-body}} + U_B^{3\text{-body}}]N_B^2}. \end{aligned} \quad (36)$$

Figure 9(a) shows that this improved result well approaches κ_T in the strong-coupling BEC regime [$(k_F a_s)^{-1} \gtrsim +1$]. This

confirms the sizable contribution of the three-body molecular interaction to κ_T in this regime. We briefly note that a similar three-body correction has also recently been discussed in a Bose-Fermi mixture [87].

As mentioned previously, Ref. [81] has found from self-energy analyses that the SCTMA scheme actually has a correction to the well-known two-body molecular interaction in Eq. (14). Our result is consistent with this statement in the sense that this correction is just equal to $U_B^{3\text{-body}}$ in Eq. (35), being obtained from the vertex correction to the isothermal compressibility. This is again a consequence of the consistent treatment of the self-energy Σ and the three-point vertex correction Λ in our theory.

The improved molecular scattering length $a_B = [2 - 0.842]a_s = 1.158a_s$ obtained from $U_B^{2\text{-body}} + U_B^{3\text{-body}}$ is, however, still larger than the exact value $a_B = 0.6a_s$ [67,68]. This means that the SCTMA underestimates κ_T in the BEC regime. Since κ_T in the SCTMA can explain the recent experiment on a ${}^6\text{Li}$ unitary Fermi gas [34] (see Fig. 8), the observation of κ_T away from the unitary limit would be helpful to see where in the BEC side one needs to improve the SCTMA.

Here, we compare our result ($a_B = 1.158a_s$) with the values of a_B obtained by various diagrammatic approaches. References [15,16] examined a_B in the SCTMA to obtain $a_B = 2a_s$. Reference [81] studied the self-energy in the SCTMA to obtain the same result as ours. Reference [66] considered the lowest-order molecular interaction in Eq. (14), as well as its multiscattering processes, giving $a_B \simeq 0.75a_s$; however, the three-body correction in Eq. (35) is ignored in this approach. Reference [72] included all diagrammatic contributions to a_B to obtain the exact value $a_B \simeq 0.6a_s$ [67,68]. Our two-body ($U_B^{2\text{-body}}$) and three-body ($U_B^{3\text{-body}}$) scattering processes can be seen in Figs. 4(a) and 4(b) in Ref. [72], respectively. Although our result ($a_B = 1.158a_s$) is closer to the exact value $a_B \simeq 0.6a_s$ than $a_B = 2a_s$, to further improve this, we need to include higher-order corrections, as well as multiscattering processes, beyond the SCTMA.

Before ending this section, we note that, although $\kappa_T^{(3)}$ in Eq. (24) also involves contributions from higher-body molecular interactions $U_B^{l\text{-body}}$ ($l \geq 4$), their contributions are all $O(a_s^n)$ ($n \geq 2$), so that they can be ignored compared to $U_B^{2\text{-body}} \propto a_s$ and $U_B^{3\text{-body}} \propto a_s$, when $(k_F a_s)^{-1} \gg 1$. [Although the corresponding diagrams are not shown in Fig. 10(a), for reference, we show in Fig. 11 a four-body molecular interaction and the corresponding diagram involved in $\kappa_T^{(3)}$.] However, it is still unclear whether such higher-body molecular interactions are really irrelevant or their contributions are actually $O(a_s)$ in a more sophisticated strong-coupling theory beyond the SCTMA, which remains as our future problem. Since the effects of multibody molecular interactions, as well as their multiscattering processes, should be all taken into account in the exact molecular scattering $a_B = 0.6a_s$ [72], in order to assess the importance of higher-body molecular interactions, it would be useful to diagrammatically decompose this exact calculation into contributions from l -body molecular interactions. Such analyses might also be helpful in improving the SCTMA so that it can deal

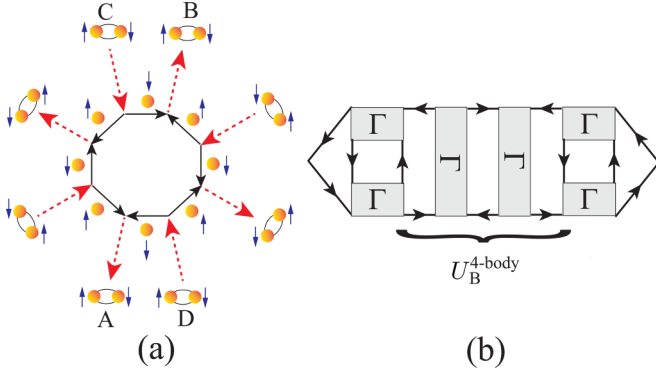


FIG. 11. (a) Four-body molecular interaction. (b) Diagram involving the effects of the four-body molecular interaction on κ_T in the SCTMA. In panel (b), the four-body contribution $U_B^{4\text{-body}}$ is obtained from panel (a) by connecting the two outgoing molecular lines “A” and “B” to the incident lines “C” and “D,” respectively.

with the strong BEC regime in a more quantitative manner.

IV. SUMMARY

To summarize, we have discussed the isothermal compressibility κ_T in the BCS-BEC crossover regime of an ultracold Fermi gas above T_c . Within the framework of the self-consistent T -matrix approximation (SCTMA), we have computed κ_T in the whole BCS-BEC crossover region. Using the property that this thermodynamic quantity is sensitive to the strength of a Bose-Bose repulsion, we evaluated molecular interactions in the strong-coupling BEC regime.

We showed that κ_T monotonically increases with decreasing the temperature in the whole BCS-BEC crossover region, but still converges at T_c . In the strong-coupling BEC regime where most Fermi atoms form tightly bound molecular bosons, this convergence is attributed to molecular interactions mediated by unpaired Fermi atoms: not only a two-body molecular interaction, but also a three-body one sizably affects this thermodynamic quantity. While the former gives the molecular scattering length $a_B = 2a_s$ (which is well known in the SCTMA), the latter corrects this value to $a_B = 1.158a_s$. This result is consistent with the recent work [81], where the same modified molecular scattering length is obtained from the analysis of the SCTMA self-energy.

As a remaining future problem, although we have clarified the importance of two- and three-body components of molecular interactions in this paper, we still need to examine whether higher-body components are irrelevant or they also sizably affect κ_T , when one goes beyond the SCTMA. For this problem, it would be helpful to decompose the exact calculation (which gives $a_B = 0.6a_s$) into the contributions from such multibody molecular interactions.

In this paper, we have indirectly assessed the effects of the three-body molecular interaction through the correction to the two-body component. Thus it would also be an interesting future challenge to explore a physical quantity which is more directly affected by multibody molecular interactions.

Since molecular correlations have so far mainly been discussed within the two-body level in ultracold Fermi gases, our results would contribute to the further development of this research field.

ACKNOWLEDGMENTS

We thank M. Zwierlein for providing us with his experimental data shown in Fig. 8. We also thank R. Hanai and D. Inotani for discussions. D.K. was supported by JST CREST (Grant No. JPMJCR1673) and JST FOREST (Grant No. JPMJFR202T). K.M. was supported by a Grant-in-Aid for JSPS fellows (Grant No. 21J14011). H.T. was supported by a Grant-in-Aid for JSPS fellows (Grant No. 17J03975) and a Grant-in-Aid for Early-Career Scientists (Grant No. 22K13981). Y.O. was supported by a Grant-in-aid for Scientific Research from MEXT and JSPS in Japan (Grants No. JP18K11345, No. JP18H05406, No. JP19K03689, and No. JP22K03486).

APPENDIX A: COMPUTATIONAL METHOD TO DETERMINE $\Sigma(p, i\omega_n)$ IN SCTMA

In this Appendix, we explain how to self-consistently compute the SCTMA self-energy $\Sigma(p, i\omega_n)$ in Eq. (11) from Eqs. (9), (12), and (13). For this purpose, we make use of the Fourier transform technique [16,43] in this paper: to avoid computing the momentum and Matsubara-frequency summations in Eqs. (11) and (13), we change the variables from “momentum and Matsubara frequency” to “real space (\mathbf{r}) and imaginary time (τ)” by the Fourier transformation,

$$f(\mathbf{r}, \tau) = T \sum_{\mathbf{p}, \zeta_n} e^{i\mathbf{p}\cdot\mathbf{r} - i\zeta_n\tau} f(\mathbf{p}, i\zeta_n), \quad (\text{A1})$$

$$f(\mathbf{p}, i\zeta_n) = \int_0^{1/T} d\tau \int d\mathbf{r} e^{-i\mathbf{p}\cdot\mathbf{r} + i\zeta_n\tau} f(\mathbf{r}, \tau), \quad (\text{A2})$$

where ζ_n is the fermion or boson Matsubara frequency. Equations (11) and (13) are Fourier transformed as, respectively,

$$\Sigma(\mathbf{r}, \tau) = \Gamma(\mathbf{r}, \tau)G(-\mathbf{r}, -\tau), \quad (\text{A3})$$

$$\Pi(\mathbf{r}, \tau) = G(\mathbf{r}, \tau)^2. \quad (\text{A4})$$

Because Eqs. (9), (12), (A3), and (A4) no longer have any summation, we can quickly compute these. Using this advantage, we self-consistently determine the SCTMA self-energy following the flowchart in Fig. 12. For the Fourier transformation, we employ the spline interpolation-based Fourier-transform technique, developed in Refs. [16,43].

APPENDIX B: DIVERGENCE OF TMA ISOTHERMAL COMPRESSIBILITY AT T_c

The TMA self-energy Σ_{TMA} is obtained from Eq. (11) by replacing all the dressed Green’s function G with the bare one G_0 . Evaluating the TMA isothermal compressibility κ_T^{TMA}

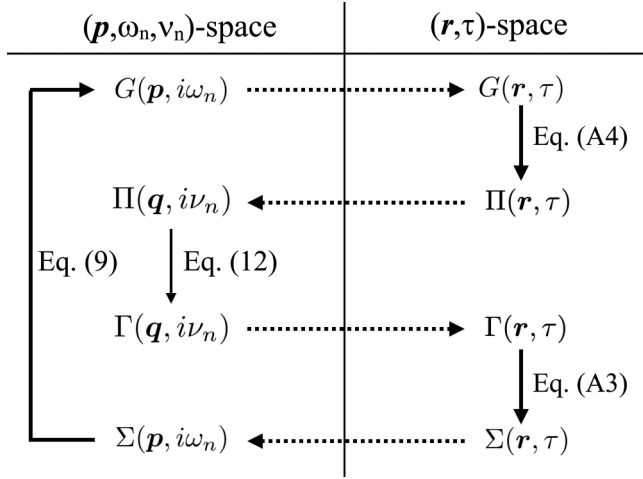


FIG. 12. Flowchart about self-consistent calculation of SCTMA self-energy $\Sigma(\mathbf{p}, i\omega_n)$ in Eq. (11). The solid arrow means the operation of the equation written beside the arrow. The dashed arrow denotes the Fourier transformation in Eqs. (A1) and (A2). We numerically repeat the “calculation loop” in this flowchart, until $\Sigma(\mathbf{p}, i\omega_n)$ is self-consistently determined.

from Eq. (17), we obtain

$$\begin{aligned} \kappa_T^{\text{TMA}} = & -\frac{2T}{N^2} \sum_{\mathbf{p}, \omega_n} G_{\text{TMA}}^2(\mathbf{p}, i\omega_n) \\ & -\frac{2T^2}{N^2} \sum_{\mathbf{p}, \omega_n} \sum_{\mathbf{q}, \nu_n} G_{\text{TMA}}^2(\mathbf{p}, i\omega_n) \\ & \times \Gamma_{\text{TMA}}(\mathbf{q}, i\nu_n) G_0^2(\mathbf{q} - \mathbf{p}, i\nu_n - i\omega_n) \\ & + \frac{4T^3}{N^2} \sum_{\mathbf{p}, \omega_n} \sum_{\mathbf{p}', \omega'_n} \sum_{\mathbf{q}, \nu_n} G_{\text{TMA}}^2(\mathbf{p}, i\omega_n) \\ & \times G_0(\mathbf{q} - \mathbf{p}, i\nu_n - i\omega_n) \Gamma_{\text{TMA}}^2(\mathbf{q}, i\nu_n) \\ & \times G_0^2(\mathbf{p}', i\omega'_n) G_0(\mathbf{q} - \mathbf{p}', i\nu_n - i\omega'_n), \quad (\text{B1}) \end{aligned}$$

where the single-particle thermal Green’s function G_{TMA} involves the TMA self-energy Σ_{TMA} and Γ_{TMA} is given by Eq. (12) with G being replaced with G_0 . At the TMA superfluid phase-transition temperature T_c^{TMA} , the gapless particle-particle scattering matrix behaves as $\Gamma_{\text{TMA}}(\mathbf{q}, 0) \sim 1/q^2$, so that the \mathbf{q} summation in the last term in Eq. (B1), as well as the resulting $\kappa_T^{\text{TMA}}(T_c^{\text{TMA}})$, always diverges over the entire BCS-BEC crossover region.

Using this singular behavior of $\Gamma_{\text{TMA}}(\mathbf{q}, i\nu_n)$, we only retain the last term in Eq. (B1), to give

$$\kappa_T^{\text{TMA}}(T_c^{\text{TMA}}) \simeq \frac{\alpha_L^{\text{TMA}} \alpha_R^{\text{TMA}}}{N^2} T \sum_{\mathbf{q}, \nu_n} \Gamma_{\text{TMA}}^2(\mathbf{q}, i\nu_n). \quad (\text{B2})$$

Here,

$$\alpha_L^{\text{TMA}} = 2T \sum_{\mathbf{p}, \omega_n} G_{\text{TMA}}^2(\mathbf{p}, i\omega_n) G_0(-\mathbf{p}, -i\omega_n) \quad (\text{B3})$$

and

$$\alpha_R^{\text{TMA}} = 2T \sum_{\mathbf{p}, \omega_n} G_0^2(\mathbf{p}, i\omega_n) G_0(-\mathbf{p}, -i\omega_n) \quad (\text{B4})$$

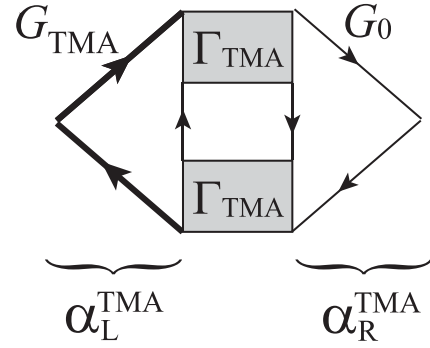


FIG. 13. Diagrammatic representation of the last term in Eq. (B1). The thick (thin) solid line is the TMA (bare) Green’s function. α_L^{TMA} and α_R^{TMA} , respectively, represent the left and right triangular parts in this diagram. Γ_{TMA} is the TMA particle-particle scattering matrix.

describe the left and right triangular vertex parts in Fig. 13, respectively. The product $\alpha_L^{\text{TMA}} \alpha_R^{\text{TMA}}$ is numerically found to change its sign at $(k_F a_s)^{-1} \simeq -0.79$, leading to the sign change of $\kappa_T^{\text{TMA}}(T_c^{\text{TMA}})$ seen in Fig. 7(b).

APPENDIX C: EVALUATION OF THE NUMBER \tilde{N}_B OF (QUASI)STABLE MOLECULES IN FIG. 9(b)

Deep inside the BEC regime $[(k_F a_s)^{-1} \gg 1]$, the particle-particle scattering matrix $\Gamma(\mathbf{q}, i\nu_n)$ in Eq. (12) is proportional to the single-particle Bose Green’s function [15,16,66]. Although this statement is, exactly speaking, only valid for the extreme BEC limit, it is still useful to approximately estimate the number \tilde{N}_B of (quasi)stable molecules in the strong-coupling BEC regime, by assuming a similar relation between $\Gamma(\mathbf{q}, i\nu_n)$ and the Bose Green’s function given in Eq. (30). That is, ignoring the lifetime of molecules, we determine the molecular excitation energy ω_q from the lowest-energy pole of the analytic continued particle-particle scattering matrix $\Gamma(\mathbf{q}, i\nu_n \rightarrow \omega_q + i\delta)$:

$$0 = 1 + \frac{4\pi a_s}{m} \left[\text{Re}[\Pi(\mathbf{q}, i\nu_n \rightarrow \omega_q + i\delta)] - \sum_{\mathbf{p}} \frac{1}{2\varepsilon_{\mathbf{p}}} \right]. \quad (\text{C1})$$

Here, we have ignored the imaginary part of $\Pi(\mathbf{q}, i\nu_n \rightarrow \omega_q + i\delta)$, for simplicity.

In the TMA, as well as the strong-coupling theory developed by Nozières and Schmitt-Rink (NSR) [13,21,61], the continuum spectrum of $\Pi(\mathbf{q}, i\nu_n \rightarrow \omega + i\delta)$, which physically describes Fermi excitations being accompanied by the dissociation of molecules, has the clear threshold energy,

$$\omega_{\text{th}} = \frac{q^2}{4m} + 2|\mu|, \quad (\text{C2})$$

in the BEC regime (where $\mu < 0$). In this case, we can unambiguously determine the molecular dispersion from the isolated pole below this threshold.

In contrast, the continuum spectrum does not have such a clear threshold in the SCTMA, because of the self-energy in the dressed Green’s function G involved in the pair-correlation function Π . Thus, in this paper, we approximately employ the

threshold energy in Eq. (C2) and only retain poles below ω_{th} , in order to distinguish between molecular states and Fermi excitations. Then, simply treating the molecule as a free boson, we estimate the number \tilde{N}_B of (quasi)stable molecules at T_c as

$$\tilde{N}_B = \sum_q \frac{1}{e^{\omega_q/T_c} - 1}. \quad (\text{C3})$$

We briefly note that the above technique has been used to evaluate \tilde{N}_B , as well as the contribution N_{scatt} from the

scattering states to the number N of Fermi atoms, in the NSR theory [61]. Within the NSR scheme, the molecular states are stable with an infinite lifetime.

APPENDIX D: DERIVATION OF EQ. (35)

We carry out the Matsubara frequency summations of ω_n and ω'_n in Eq. (35), by substituting Eq. (30) into this equation.

Approximately setting $e^{\mu/T} = 0$ (because $\mu \rightarrow -\infty$ in the BEC limit), one has $U_B^{3\text{-body}} = U_B^{3\text{-body}(1)} + U_B^{3\text{-body}(2)}$, where

$$U_B^{3\text{-body}(1)} = \frac{1}{16} \left(\frac{8\pi}{m^2 a_s} \right)^2 \sum_{\mathbf{p}, \mathbf{p}'} \frac{1}{\xi_p^2 \xi_{p'}^2} \Gamma(\mathbf{p} + \mathbf{p}', -\xi_p - \xi_{p'}), \quad (\text{D1})$$

$$U_B^{3\text{-body}(2)} = \left(\frac{8\pi}{m^2 a_s} \right)^3 \sum_{\mathbf{p}, \mathbf{q}} n_B(\varepsilon_q^B) \left[\frac{1}{\xi_p [\xi_p + \xi_{q-p} - \varepsilon_q^B]^3 [\xi_p - \xi_{q-p} - \varepsilon_q^B]} + \frac{1}{2\xi_p [\xi_p + \xi_{q-p} - \varepsilon_q^B]^2 [\xi_p - \xi_{q-p} - \varepsilon_q^B]^2} \right. \\ \left. + \frac{1}{4\xi_p^2 [\xi_p + \xi_{q-p} - \varepsilon_q^B]^2 [\xi_p - \xi_{q-p} - \varepsilon_q^B]} - \frac{1}{4\xi_{q-p}^2 [\xi_p + \xi_{q-p} + \varepsilon_q^B] [\xi_p - \xi_{q-p} - \varepsilon_q^B]^2} \right]. \quad (\text{D2})$$

Here, $n_B(\varepsilon_q^B) = [e^{\varepsilon_q^B/T} - 1]^{-1}$ is the Bose distribution function.

In Eq. (D1), we approximately set $\mu \simeq -1/(2ma_s^2)$, as well as change the variables \mathbf{p} and \mathbf{p}' as $\mathbf{p} = \mathbf{k}/a_s$ and $\mathbf{p}' = \mathbf{k}'/a_s$. Then, we have

$$U_B^{3\text{-body}(1)} = -\frac{4\pi a_s}{m} \frac{8}{\pi^2} \int_0^\infty k^2 dk \int_0^\infty k'^2 dk' \int_{-1}^1 d \cos \theta \\ \times \frac{1}{[k^2 + 1]^2} \frac{1}{[k'^2 + 1]^2} \\ \times \frac{1}{\sqrt{\frac{3}{4}[k^2 + k'^2] + \frac{kk' \cos \theta}{2} + 2 - 1}}, \quad (\text{D3})$$

where θ is the angle between \mathbf{k} and \mathbf{k}' . Numerically evaluating the integrals in Eq. (D3), we obtain

$$U_B^{3\text{-body}(1)} \simeq -\frac{4\pi(0.842a_s)}{2m}. \quad (\text{D4})$$

For the \mathbf{q} summation in Eq. (D2), because the Bose distribution function $n_B(\varepsilon_q^B)$ diverges at $\mathbf{q} = 0$, we approximately

set $\mathbf{q} = 0$ in this equation except for ε_q^B in the Bose distribution function. Again setting $\mu = -1/(2ma_s^2)$, one obtains

$$U_B^{3\text{-body}(2)} \simeq -\frac{3}{16} \left(\frac{8\pi}{m^2 a_s} \right)^3 \sum_q n_B(\xi_q^B) \sum_p \frac{1}{\xi_p^5} \\ = -\frac{15\pi^2 a_s^4 N}{m}. \quad (\text{D5})$$

In obtaining the last expression in Eq. (D5), the molecular number $\sum_q n_B(\varepsilon_q^B)$ at T_c is approximated to half the number $N/2$ of Fermi atoms (because all N Fermi atoms form Bose molecules in the BEC limit).

While $U_B^{3\text{-body}(1)} = O(a_s)$, $U_B^{3\text{-body}(2)} = O(a_s^4)$, so that the former is dominant in the BEC regime. Only retaining the former, we reach

$$U_B^{3\text{-body}} = -\frac{4\pi(0.842a_s)}{M_B}, \quad (\text{D6})$$

where $M_B = 2m$.

- [1] J. R. Schrieffer, *Theory of Superconductivity* (Westview Press, Boulder, CO, 1999).
 [2] C. A. Regal, M. Greiner, and D. S. Jin, *Phys. Rev. Lett.* **92**, 040403 (2004).
 [3] M. W. Zwierlein, C. A. Stan, C. H. Schunck, S. M. F. Raupach, A. J. Kerman, and W. Ketterle, *Phys. Rev. Lett.* **92**, 120403 (2004).
 [4] J. Kinast, S. L. Hemmer, M. E. Gehm, A. Turlapov, and J. E. Thomas, *Phys. Rev. Lett.* **92**, 150402 (2004).
 [5] M. Bartenstein, A. Altmeyer, S. Riedl, S. Jochim, C. Chin, J. H. Denschlag, and R. Grimm, *Phys. Rev. Lett.* **92**, 203201 (2004).

- [6] W. Ketterle and M. W. Zwierlein, in *Ultra-Cold Fermi Gases*, edited by M. Inguscio, W. Ketterle, and C. Salomon (IOS Press, Amsterdam, 2008).
 [7] I. Bloch, J. Dalibard, and W. Zwerger, *Rev. Mod. Phys.* **80**, 885 (2008).
 [8] Q. Chen, J. Stajic, S. Tan, and K. Levin, *Phys. Rep.* **412**, 1 (2005).
 [9] S. Giorgini, L. P. Pitaevskii, and S. Stringari, *Rev. Mod. Phys.* **80**, 1215 (2008).
 [10] *The BCS-BEC Crossover and the Unitary Fermi Gas*, edited by W. Zwerger (Springer, Berlin, 2012).

- [11] D. M. Eagles, *Phys. Rev.* **186**, 456 (1969).
- [12] A. J. Leggett, in *Modern Trends in the Theory of Condensed Matter*, edited by A. Pekalski and J. A. Przystawa (Springer, Berlin, 1980), p. 13.
- [13] P. Nozières and S. Schmitt-Rink, *J. Low Temp. Phys.* **59**, 195 (1985).
- [14] C. A. R. Sá de Melo, M. Randeria, and J. R. Engelbrecht, *Phys. Rev. Lett.* **71**, 3202 (1993).
- [15] R. Haussmann, *Z. Phys. B* **91**, 291 (1993).
- [16] R. Haussmann, *Phys. Rev. B* **49**, 12975 (1994).
- [17] M. Randeria, in *Bose-Einstein Condensation*, edited by A. Griffin, D. W. Snoke, and S. Stringari (Cambridge University Press, Cambridge, UK, 1995), p. 355.
- [18] E. Timmermans, K. Furuya, P. W. Milonni, and A. K. Kerman, *Phys. Lett. A* **285**, 228 (2001).
- [19] M. Holland, S. J. J. M. F. Kokkelmans, M. L. Chiofalo, and R. Walser, *Phys. Rev. Lett.* **87**, 120406 (2001).
- [20] F. Pistolesi and G. C. Strinati, *Phys. Rev. B* **49**, 6356 (1994).
- [21] Y. Ohashi and A. Griffin, *Phys. Rev. Lett.* **89**, 130402 (2002).
- [22] C. Chin, R. Grimm, P. Julienne, and E. Tiesinga, *Rev. Mod. Phys.* **82**, 1225 (2010).
- [23] J. Kinast, A. Turlapov, J. E. Thomas, Q. Chen, J. Stajic, and K. Levin, *Science* **307**, 1296 (2005).
- [24] A. Altmeyer, S. Riedl, C. Kohstall, M. J. Wright, R. Geursen, M. Bartenstein, C. Chin, J. H. Denschlag, and R. Grimm, *Phys. Rev. Lett.* **98**, 040401 (2007).
- [25] J. T. Stewart, J. P. Gaebler, and D. S. Jin, *Nature (London)* **454**, 744 (2008).
- [26] L. Luo and J. E. Thomas, *J. Low Temp. Phys.* **154**, 1 (2009).
- [27] J. P. Gaebler, J. T. Stewart, T. E. Drake, D. S. Jin, A. Perali, P. Pieri, and G. C. Strinati, *Nat. Phys.* **6**, 569 (2010).
- [28] S. Nascimbène, N. Navon, K. J. Jiang, F. Chevy, and C. Salomon, *Nature (London)* **463**, 1057 (2010).
- [29] N. Navon, S. Nascimbène, F. Chevy, and C. Salomon, *Science* **328**, 729 (2010).
- [30] C. Cao, E. Elliott, J. Joseph, H. Wu, J. Petricka, T. Schäfer, and J. E. Thomas, *Science* **331**, 58 (2011).
- [31] C. Sanner, E. J. Su, A. Keshet, W. Huang, J. Gillen, R. Gommers, and W. Ketterle, *Phys. Rev. Lett.* **106**, 010402 (2011).
- [32] A. Sommer, M. Ku, G. Roati, and M. W. Zwierlein, *Nature (London)* **472**, 201 (2011).
- [33] A. Sommer, M. Ku, and M. W. Zwierlein, *New J. Phys.* **13**, 055009 (2011).
- [34] M. J. H. Ku, A. T. Sommer, L. W. Cheuk, and M. W. Zwierlein, *Science* **335**, 563 (2012).
- [35] E. Elliott, J. A. Joseph, and J. E. Thomas, *Phys. Rev. Lett.* **113**, 020406 (2014).
- [36] Y. Sagi, T. E. Drake, R. Paudel, R. Chapurin, and D. S. Jin, *Phys. Rev. Lett.* **114**, 075301 (2015).
- [37] J. A. Joseph, E. Elliott, and J. E. Thomas, *Phys. Rev. Lett.* **115**, 020401 (2015).
- [38] M. Horikoshi, M. Koashi, H. Tajima, Y. Ohashi, and M. Kuwata-Gonokami, *Phys. Rev. X* **7**, 041004 (2017).
- [39] S. Hoinka, P. Dyke, M. G. Lingham, J. J. Kinnunen, G. M. Bruun, and C. J. Vale, *Nat. Phys.* **13**, 943 (2017).
- [40] P. Pieri, L. Pisani, and G. C. Strinati, *Phys. Rev. B* **70**, 094508 (2004).
- [41] G. M. Bruun and H. Smith, *Phys. Rev. A* **72**, 043605 (2005).
- [42] H. Hu, X.-J. Liu, and P. D. Drummond, *Phys. Rev. A* **73**, 023617 (2006).
- [43] R. Haussmann, W. Rantner, S. Cerrito, and W. Zwerger, *Phys. Rev. A* **75**, 023610 (2007).
- [44] N. Fukushima, Y. Ohashi, E. Taylor, and A. Griffin, *Phys. Rev. A* **75**, 033609 (2007).
- [45] H. Hu, X.-J. Liu, and P. D. Drummond, *Phys. Rev. A* **77**, 061605(R) (2008).
- [46] S. Tsuchiya, R. Watanabe, and Y. Ohashi, *Phys. Rev. A* **80**, 033613 (2009).
- [47] Q. Chen and K. Levin, *Phys. Rev. Lett.* **102**, 190402 (2009).
- [48] M. Iskin and C. A. R. Sá de Melo, *Phys. Rev. Lett.* **103**, 165301 (2009).
- [49] R. Watanabe, S. Tsuchiya, and Y. Ohashi, *Phys. Rev. A* **82**, 043630 (2010).
- [50] H. Hu, X.-J. Liu, P. D. Drummond, and H. Dong, *Phys. Rev. Lett.* **104**, 240407 (2010).
- [51] P. Magierski, G. Wlazłowski, and A. Bulgac, *Phys. Rev. Lett.* **107**, 145304 (2011).
- [52] S. Tsuchiya, R. Watanabe, and Y. Ohashi, *Phys. Rev. A* **84**, 043647 (2011).
- [53] E. J. Mueller, *Phys. Rev. A* **83**, 053623 (2011).
- [54] A. Perali, F. Palestini, P. Pieri, G. C. Strinati, J. T. Stewart, J. P. Gaebler, T. E. Drake, and D. S. Jin, *Phys. Rev. Lett.* **106**, 060402 (2011).
- [55] T. Enss, R. Haussmann, and W. Zwerger, *Ann. Phys. (NY)* **326**, 770 (2011).
- [56] F. Palestini, P. Pieri, and G. C. Strinati, *Phys. Rev. Lett.* **108**, 080401 (2012).
- [57] T. Enss and R. Haussmann, *Phys. Rev. Lett.* **109**, 195303 (2012).
- [58] T. Kashimura, R. Watanabe, and Y. Ohashi, *Phys. Rev. A* **86**, 043622 (2012).
- [59] G. Wlazłowski, P. Magierski, J. E. Drut, A. Bulgac, and K. J. Roche, *Phys. Rev. Lett.* **110**, 090401 (2013).
- [60] H. Tajima, T. Kashimura, R. Hanai, R. Watanabe, and Y. Ohashi, *Phys. Rev. A* **89**, 033617 (2014).
- [61] P. van Wyk, H. Tajima, R. Hanai, and Y. Ohashi, *Phys. Rev. A* **93**, 013621 (2016).
- [62] M. Ota, H. Tajima, R. Hanai, D. Inotani, and Y. Ohashi, *Phys. Rev. A* **95**, 053623 (2017).
- [63] H. Tajima, P. van Wyk, R. Hanai, D. Kagamihara, D. Inotani, M. Horikoshi, and Y. Ohashi, *Phys. Rev. A* **95**, 043625 (2017).
- [64] D. Kagamihara, D. Inotani, and Y. Ohashi, *J. Phys. Soc. Jpn.* **88**, 114001 (2019).
- [65] D. Kagamihara and Y. Ohashi, *J. Phys. Soc. Jpn.* **89**, 044005 (2020).
- [66] P. Pieri and G. C. Strinati, *Phys. Rev. B* **61**, 15370 (2000).
- [67] D. S. Petrov, C. Salomon, and G. V. Shlyapnikov, *Phys. Rev. Lett.* **93**, 090404 (2004).
- [68] D. S. Petrov, C. Salomon, and G. V. Shlyapnikov, *Phys. Rev. A* **71**, 012708 (2005).
- [69] Y. Ohashi, *J. Phys. Soc. Jpn.* **74**, 2659 (2005).
- [70] J. Tempere and J. T. Devreese, *J. Phys. B: At., Mol., Opt. Phys.* **39**, S57 (2006).
- [71] J. R. Engelbrecht, M. Randeria, and C. A. R. Sá de Melo, *Phys. Rev. B* **55**, 15153 (1997).
- [72] I. V. Brodsky, M. Y. Kagan, A. V. Klaptsov, R. Combescot, and X. Leyronas, *Phys. Rev. A* **73**, 032724 (2006).

- [73] C. J. Pethick and H. Smith, *Bose-Einstein Condensation in Dilute Gases* (Cambridge University Press, Cambridge, UK, 2008).
- [74] L. P. Pitaevskii and S. Stringari, *Bose-Einstein Condensation and Superfluidity* (Oxford University Press, Oxford, 2016).
- [75] J. Joseph, B. Clancy, L. Luo, J. Kinast, A. Turlapov, and J. E. Thomas, *Phys. Rev. Lett.* **98**, 170401 (2007).
- [76] J. Fujita and H. Miyazawa, *Prog. Theor. Phys.* **17**, 360 (1957).
- [77] J. Carlson, S. Gandolfi, F. Pederiva, S. C. Pieper, R. Schiavilla, K. E. Schmidt, and R. B. Wiringa, *Rev. Mod. Phys.* **87**, 1067 (2015).
- [78] K. Tsubakihara and A. Ohnishi, *Nucl. Phys. A* **914**, 438 (2013).
- [79] A. Perali, P. Pieri, G. C. Strinati, and C. Castellani, *Phys. Rev. B* **66**, 024510 (2002).
- [80] We note that, in contrast to the case of the normal state, the TMA can describe the molecular interaction in the superfluid phase, which comes from the off-diagonal anomalous Green's function. The resulting TMA sound velocity of the Goldstone mode in the BEC regime coincides with the velocity of the Bogoliubov phonon in an assumed Bose superfluid with the molecular scattering length $a_B = 2a_s$.
- [81] M. Pini, P. Pieri, and G. C. Strinati, *Phys. Rev. B* **99**, 094502 (2019).
- [82] D. J. Thouless, *Ann. Phys. (NY)* **10**, 553 (1960).
- [83] R. Hanai and Y. Ohashi, *Phys. Rev. A* **90**, 043622 (2014).
- [84] We note that the number \tilde{N}_B of (quasi)stable molecules does *not* involve the contribution ($\equiv N_{\text{scatt}}$) from the so-called scattering states [13,21,61] that physically describe fluctuating Cooper pairs. While the (quasi)stable molecules only appear in the strong-coupling BEC side [$(k_F a_s)^{-1} \lesssim 0.5$, where $\mu < 0$], N_{scatt} first continuously increases with increasing the interaction strength in the BCS regime, reflecting the enhancement of pairing fluctuations; however, N_{scatt} decreases to eventually disappear deep inside the BEC regime where system properties are dominated by (quasi)stable molecules. Since the molecular states obtained in the SCTMA have a small but nonzero decay rate (which is, however, ignored in calculating \tilde{N}_B ; see Appendix C), we call them “(quasi)” stable molecules in this paper.
- [85] We note that, as seen in Fig. 5(a), the SCTMA does not give the expected hump in T_c . Regarding this, in a more sophisticated theory which can describe this expected structure, when one moves along this T_c line from the weak- to strong-coupling regime, the (quasi)stable molecules should also start to appear in the BEC side, and their effects on κ_T would be similar to the SCTMA case. Thus, unless the hump in κ_T seen in Fig. 9(a) has nothing to do with the appearance of molecules, we expect that this structure still remains, even when the hump in T_c is taken into account. However, to confirm this expectation, although the TMA [79] as well as the strong-coupling theory developed by Nozières and Schmitt-Rink (NSR) [13] give a hump in T_c around $(k_F a_s)^{-1} \approx 0.4\text{--}0.8$ [81], we cannot use these theories, because they unphysically give diverging $\kappa_T(T_c)$, due to the ignorance of the molecular interaction. It remains as one of our future problems to clarify how the detailed behavior of T_c in the BCS-BEC crossover region affects the hump in κ_T .
- [86] We note that the Hartree self-energy in Fig. 4(c) does not appear in G_B at T_c . This is because it is canceled out by the Bose chemical potential to give gapless Bose excitations at the superfluid phase transition.
- [87] K. Manabe and Y. Ohashi, *Phys. Rev. A* **103**, 063317 (2021).